ELSEVIER

Biophysical Chemistry 79 (1999) 41–53

Biophysical Chemistry

Simulation of the distribution and diffusion of a rigid amphipathic particle embedded in a model membrane

M.X. Fernandes[a], M.L. Huertas[b], M.A.R.B. Castanho[a,c], J. García de la Torre[b,*]

[a] *Departamento de Química e Bioquímica, Faculdade de Cências da UL, Bl. C1-5o, Campo Grande, 1700 Lisboa, Portugal*
[b] *Departamento de Química Física, Facultad de Química, Universidad de Murcia, 30071 Murcia, Spain*
[c] *Centro de Química Física Molecular, Complexo I -IST, 1096 Lisboa Codex, Portugal*

Received 26 October 1998; received in revised form 17 March 1999; accepted 17 March 1999

Abstract

We simulate, by Brownian dynamics, the distribution, orientation and diffusion of a rigid molecule, represented as a dumbbell, with amphipathic nature, embedded in a model membrane. The significant features of a biological membrane are reproduced by means of a Maier–Saupe orienting potential, an enclosing potential and a lipophobic potential. We also evaluate the equilibrium quantities, such as order parameter, and dynamic features, such as rotational or translational diffusivity, of the embedded molecule in terms of the system parameters and compare the obtained results with those obtained from model independent theory.

Keywords: BD simulation; Dynamics; Model membrane; Amphipathic probe

1. Introduction

Biological membranes are the selective envelope of cells, and they play many relevant roles and functions. These biological functions are intrinsically based on the structure of the membrane. The amphipathic nature and the transversal characteristic profile of a biomembrane, with the typical polar head groups and hydrocarbon chains organisation, is well known as being essential for performing its function. Insight on membrane physical features, both structural and dynamic, is therefore of extreme importance for understanding biological function, most particularly those related to the amphipathic nature of the membrane.

A fruitful approach to the knowledge of membrane structure and dynamics consists of observing the properties of fluorescent probe molecules embedded in the membrane [1]. Some widely

* Corresponding author. Tel.: +34-968-364148; e-mail: jgt@fcu.um.es

0301-4622/99/$ - see front matter
PII: S0301-4622(99)00039-9

used probes, particularly 1,6-diphenyl-1,3,5-hexatriene (DPH) are fully apolar, hydrophobic molecules, which intercalate within the hydrocarbon region of the lipid bilayer [2,3]. However, there are other probes having the interesting feature of being amphipathic, with a polar, hydrophilic end and an apolar hydrocarbon tail, like the lipid molecules themselves. Particularly, *trans*-parinaric acid, *t*-PnA [4–6] and, more recently, *trans*- and *cis*-octadecapentanoic acid [7] have been explored, by means of fluorescence spectroscopy, to determine physical properties and organisation of lipid bilayers. Using dynamic spectroscopic techniques [8] such as fluorescence anisotropy decay [7], the orientational distribution and the dynamics of the probe molecules can be monitored. Other spectroscopic techniques are also available for this purpose [9].

Another interesting case is provided by membrane α-helical peptides having a more or less rigid central part which is hydrophobic and interacts favourably with the lipidic region, while one or the two ends are polar, hydrophilic and tend to be at the lipid–water interface [9–11]. An example that bears a special resemblance with the model that we will describe below is alamethicin whose C-terminus protrudes well outside the hydrocarbon region, being bathed by the aqueous phase (see Figure 1 in reference [11]).

In the past decade, the computer simulation of lipid bilayers has gained recognition as a powerful approach for the structural and dynamic study of biomembranes. An emerging tool for the simulation of these systems is the molecular dynamics technique (see van der Ploeg and Berendsen [12], Lopez Cascales et al. [13] for a more recent work, and Tieleman et al. [14] for a review). This technique offers the advantage of describing the system with atomic detail, and is being used nowadays in a number of laboratories, including our own [15–18]. The major disadvantage of molecular dynamics is the limited time scale accessible, usually in the order of a few nanoseconds. For the specific situation of distribution and dynamics of probes and other penetrant molecules, the possibilities and limitations of molecular dynamics have been illustrated [18–20]. Another related technique is stochastic dynamics simulation, employed mainly by Pastor and co-workers [20–22] for molecular models with nearly atomic detail, which still restricts the time scale of the results. On the other hand, theories have been devised for the analysis of rotational dynamics of molecules in orienting environments [23,24]. Their results are notably helpful because they are model independent, requiring only the order parameters and the rotational diffusion coefficients of the probe molecule. The theories are developed from simple physical models of the probe–membrane system, and the obtention of analytical results made it necessary to make some approximations in the theoretical treatment.

The starting point in the interpretation of experimental observations on membrane research data is the knowledge of the individual contributions of different existing bilayer driving forces such as orientation, fluidity or miscibility. To do this it is commonly assumed that probe molecules experience potentials imposed by the surrounding lipid molecules. However, links between complex dynamic behaviour of probes, monitored by different techniques, individual driving forces and probe localisation are still missing. The resolution of this problem demands an approach in which the individual contributions can be followed. Conversely to experimentation, this can be done in a straightforward way taking hand of Brownian dynamics simulation.

Recently, we have proposed [25] to represent the probe–membrane system by such simple models, whose behaviour is simulated using Brownian dynamics technique. At the cost of sacrificing somehow the molecular detail, the time scale where diffusive processes take place in biological membranes can be reached with a model that still represents well the most essential aspects of the system, such as orientational effects, diffusion in a viscous regimen, confinement, etc. This is useful not only to check the predictions of the above-mentioned theories, but also to introduce further refinements in the model system, and for the prediction of features for which no theoretical results are available. In our first publication, we considered the case of a hydrophobic probe molecule, as it could be the case of DPH. In the present paper, we extend the treatment to

the case, whose relevance has been described above, in which the embedded molecule is amphipathic [25].

2. Model and methodological features

2.1. Model, geometry and energetics

The system that we consider consists of a rigid probe molecule moving in the interior of a membrane of a given thickness. The probe is assumed to have an amphipathic nature and a somewhat elongated shape, of which one of the ends is essentially hydrophobic and the other one is lipophobic.

The model used to represent this system is based on that proposed by Huertas et al. [25] for a purely hydrophobic probe, with the appropriate modification for an amphipathic molecule. If the probe has, approximately, an axial symmetry, it can be represented by a simple model, the dumbbell, formed by two spheres joined by a frictionless connector. One of these spheres is hydrophobic and the other one is lipophobic. The probe's motion is restricted to the boundaries of the membrane which has a finite dimension along the z-axis.

The order feature of the membrane is represented by means of an orienting potential. This interaction between the probe and the membrane is described by a Maier–Saupe potential, which reads

$$V_{\text{orient}}(\theta) = -(3/2)kTK_{\theta}(\cos^2\theta - 1)$$

where θ is the angle formed by the z-axis and the connector axis that joins the two beads. The z-axis coincides with the transverse direction of the membrane. kT is the thermal energy term and K_{θ} is a dimensionless constant that determines the magnitude of the orienting potential, V_{orient}. This potential is maximum for an orientation perpendicular to the transverse plane of the membrane, meaning $\theta = \pi/2$, and minimum for a parallel orientation, meaning $\theta = 0$ or $\theta = \pi$. However, a modification in the treatment of Huertas et al. [25] is pertinent. Only the hydrophobic part of the environment which surrounds the probe molecule, i.e. meaning the lipid bilayer itself, but not the aqueous region, has an orienting effect. In order to represent this, we introduce a factor $f \leq 1$ in $V_{\text{orient}}(\theta)$:

$$V_{\text{orient}}(\theta) = -(3/2)kTK_{\theta}f(\cos^2\theta - 1) \quad (1)$$

where f is the fraction of the probe length that at a given time is within the lipidic region.

The width of the membrane in the z direction is h. Specifically the membrane boundaries have z co-ordinates of $-z_0$ and z_0, with $z_0 = h/2$. The hydrophobic sphere of the probe molecule can not trespass the boundaries of the membrane towards the exterior, meaning that $|z_1| \leq z_0$, where z_1 is the z co-ordinate of the hydrophobic bead. To express this repulsion of the hydrophobic bead by the polar surfaces of the membrane in a continuous form we use a enclosing potential, V_{encl}, that reads

$$V_{\text{encl}}(z_1) = kTK_z/(z_0^2 - z_1^2) \quad (2)$$

where K_z is the constant that determines the magnitude of the enclosing potential. V_{encl} is rather low in the centre of the membrane and rapidly assumes high values as it approaches the polar boundaries of the membrane.

The lipophobic sphere of the probe is repelled by the apolar interior of the membrane. This sphere can trespass the polar boundaries of the membrane towards the exterior (which in the real case would be an aqueous region) and can, of course, stay in the interior of the membrane. To represent this lipophobic potential, V_{lipo}, in a continuous form, we take hand of the following expression

$$V_{\text{lipo}}(z_2) = kTK_{\text{lipo}}\cos^2(z_2\pi/h) \quad \text{if } |z_2| \leq z_0$$
$$\text{and} \quad (3)$$
$$V_{\text{lipo}}(z_2) = 0 \quad \text{if } |z_2| > z_0$$

where K_{lipo} is the constant that determines the magnitude of the lipophobic potential and z_2 is the z co-ordinate of the lipophobic sphere of the probe. This potential has a maximum in the interior of the membrane and reaches it's minimum

at the boundaries and at the exterior of the membrane. In addition to its simplicity, this potential has an important feature for our purposes: at the boundary, not only the potential but also its first derivative $(dV_{lipo}/dz_2)_{z_0} = 0$, are continuous, which assures the continuity of the forces.

The system and the profiles of the enclosing and lipophobic potentials are represented in Fig. 1.

2.2. Dynamic features

The amphipathic probe is regarded as a dumbbell constituted by two frictional elements, the two spheres, and a frictionless connector with dimension l. The length of the connector is not fixed but instead quasi-rigid acting as a spring with a Hookean potential, $V(b) = kTH(b-l)^2$, where b is the instantaneous length and l is the equilibrium value for the length. A high value of $100kT/l$ was assigned to H, the spring constant, in order to ensure that the root mean square value of b, $\langle b^2 \rangle^{1/2}$ exceeds l only by 2.5%.

The spheres, both of them with the same radii, σ, have a friction coefficient, according to Stokes law, of $\zeta_i = s\pi\eta\sigma_i$, where $s = 6$ or 4, respectively,

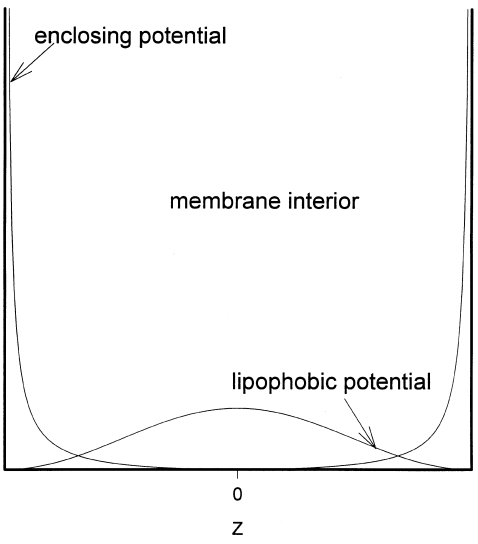

Fig. 1. Profile of enclosing and lipophobic potentials along the transverse plane of the membrane.

for stick or slip boundary conditions (the presentation of our results in terms of reduced quantities is independent of the choice of the boundary condition). In the hydrodynamic description of our system one must bear in mind that each sphere experiences different viscosities when one of them is in the aqueous phase. When hydrodynamic interaction takes place in a homogeneous fluid there is no problem since the viscosity used for the calculation of the hydrodynamic interaction tensor is well known. In our case, the hydrophobic sphere always experiences the same viscosity, η_m, but the lipophobic sphere experiences the membrane viscosity, η_m, if it is embedded in the membrane or the aqueous phase viscosity, η_a, if it is positioned outside the membrane boundaries. The supermatrix used to represent the diffusion tensor of our system has the following structure. The elements $\boldsymbol{D}_{ii}$ take the value kT/ξ_a or kT/ξ_b depending on the location of bead i. The elements $\boldsymbol{D}_{ij}$ $(i \neq j)$ take the value $kT/8\pi\eta_0 R_{12}\boldsymbol{T}_{ij}$, where R_{12} is the distance between the two spheres. We use an ad hoc modification and replace the viscosity by a weighted-average viscosity when we want to take into account the hydrodynamic interaction between the two spheres:

$$\eta_0 = (1-f)\eta_a + f\eta_m$$

where f is the fraction of the probe length within the membrane. The hydrodynamic interaction between the two spheres was taken into account in our simulation using a Oseen tensor, $\boldsymbol{T}_{ij}$ [26].

The translational and rotational coefficients can be calculated from elementary hydrodynamics [27]. When we consider hydrodynamic interaction these coefficients for a dumbbell can be numerically calculated using a bead-model, and for the case of strongest hydrodynamic interaction, corresponding to $\sigma_1 = \sigma_2 = l/2$, meaning tangent spheres, the results are for $D_t^* = 0.750$ and $D_r^{\perp *} = 1.125$, where the latest value does not include the volume correction for rotational diffusion [28], for consistency with the Brownian dynamics methodology.

The algorithm used in our simulations is the

one proposed by Ermak and McCammon [29], with the posterior correction introduced by Iniesta and Garcia de la Torre [30]. (The standard version of this algorithm, that has been used in this work, ignores a term related to the divergence of the diffusion tensor, which is usually negligible. The divergence is not exactly null if the diffusion tensor is inhomogeneous, as it happens in our case due to the change in viscosity. Anyhow, the influence of this spurious drift term in the numerical result is expected to be quite small and will not influence our conclusions.) In our simulations we use reduced quantities, that are useful for results, programming and presentation. So, lengths are reduced after division by the probe's connector equilibrium length. The unit of translational diffusion is kT/ζ and time is reduced by means of the following expression

$$t^* = (kT/\zeta l^2)t \tag{4}$$

The simulated trajectories reached the range of 100–500 units of reduced time, with a reduced time step of 10^{-4}. To give an idea of the corresponding time scale in physical units of time, let us assume a dumbbell with beads of 5 Å in diameter, and a frictionless connector with 3 Å length. In a viscous medium with $\eta_m = 2.5$ cP, 10^{-4} and 500 units of reduced time correspond, respectively, to 70 fs and 350 ns. The trajectories thus generated were statistically analysed to recover equilibrium properties calculated as averages over the trajectory. From the simulated trajectories we also recover the correlation functions, which are evaluated at discretised selected times. The numerical values of these functions are fitted with DISCRETE, a multiexponential fit procedure developed by Provencher [31,32]. The resulting fitted function has the following appearance

$$\langle P_2(t^*)\rangle = a_0 + a_a\exp(-b_a t^*) + a_b\exp(-b_b t^*) + \ldots \tag{5}$$

These amplitudes and time constants will be compared with theoretical values (vide infra).

3. Theory

3.1. Equilibrium properties

As we have a simple model for the description of our system we can derive and calculate equilibrium properties for our probe with mechanical–statistical treatment. To specify the instantaneous position of the probe molecule we need three parameters: the polar angles θ and ϕ and the position, z_1, of the hydrophobic sphere. These parameters along with the end-to-end distance determine the position of the lipophobic sphere, from which the total potential energy can be calculated. Now, the potential energy reads

$$V(z,\theta) = V_{\text{orient}}(\theta) + V_{\text{encl}}(z_1) + V_{\text{lipo}}(z_2) \tag{6}$$

where $V_{\text{orient}}(\theta)$, $V_{\text{encl}}(z_1)$ and $V_{\text{lipo}}(z_2)$ are given by Eqs. (1)–(3), respectively.

The statistical mechanic treatment must be formulated in terms of a set of as few variables as possible. Such a set can be determined by the orientational angle, θ, of the probe vector $(1 \rightarrow 2)$ and the z co-ordinate of any point in the probe axis.

$$p(\theta,z_1) = \sin\theta \mathrm{e}^{-V(z_1,\theta)/kT} \Big/ \left(\int \mathrm{d}z_1 \int \sin\theta \mathrm{e}^{-V(z_1,\theta)/kT}\mathrm{d}\theta\right) \tag{7}$$

For the amphipathic probe, it seems convenient to choose the z co-ordinate of bead 1, as it is already formulated in Eq. (7), where $p(\theta,z_1)$ includes geometrical ponderation, via $\sin\theta$, and thermodynamic ponderation, via Boltzmann factor. The range of integration are for $z_1 \in [-z_0, z_0]$ and for $\theta \in [0,\pi]$.

The potential equations are written in terms of only two variables by substituting $z_2 = z_1 + l\cos\theta$ in Eqs. (3) and (6).

The distribution function along the z axis of the hydrophobic bead is obtained integrating the last equation over all possible angles:

$$f(z_1) = \int \sin\theta e^{-V(z_1,\theta)/kT} d\theta \Big/ \left(\int dz_1 \int \sin\theta e^{-V(z_1,\theta)/kT} d\theta \right) \quad (8)$$

We can also get the angular distribution function of the probe integrating Eq. (7) over all possible z co-ordinates:

$$g(\theta) = \sin\theta \int e^{-V(z_1,\theta)/kT} dz_1 \Big/ \left(\int dz_1 \int \sin\theta e^{-V(z_1,\theta)/kT} d\theta \right) \quad (9)$$

The theoretical values of the equilibrium properties, $\langle P_2(\cos\theta)\rangle$ and $\langle P_4(\cos\theta)\rangle$, are also calculated using Eq. (7). For instance, $\langle P_2(\cos\theta)\rangle = (3\langle\cos^2\theta\rangle - 1)/2$ and it can be calculated in the following way

$$\langle\cos^2\theta\rangle = \int dz_1 \int \cos^2\theta \sin\theta e^{-V(z_1,\theta)/kT} d\theta \Big/ \left(\int dz_1 \int \sin\theta e^{-V(z_1,\theta)/kT} d\theta \right) \quad (10)$$

Any other average quantity can be obtained in the same way.

3.2. Dynamic properties

The dynamic properties that we concern about are the rotational and the translational diffusivities. The rotational dynamics of the probe can be hinted by means of the correlation function:

$$\langle P_2(t)\rangle = \langle P_2[\mathbf{u}(t)\cdot\mathbf{u}(0)]\rangle \quad (11)$$

where $\mathbf{u}(0)$ is the unitary vector along the probe's connector at one chosen initial time and $\mathbf{u}(t)$ is the same unitary vector after a time gap of t. Being unitary vectors it is clear that the result of $\mathbf{u}(t)\cdot\mathbf{u}(0)$ is just $\cos\psi$, where ψ is the angle formed between $\mathbf{u}(t)$ and $\mathbf{u}(0)$. The average present in equation (11) refers to every possible choice of the initial time. It is simple to find out that $\langle P_2(0)\rangle = 1$ and that when $t \to \infty \langle P_2(t)\rangle \to \langle P_2\rangle^2$. $\langle P_2\rangle = S$ is the equilibrium order parameter determined as mentioned above. $\langle P_2(t)\rangle$ is related to experimental features such as the decay of fluorescence anisotropy or nuclear magnetic relaxation. In any case, the multiexponential can be useful as a fitting function to represent the simulated decays.

A few theoretical approximations [23,24] predict that $\langle P_2(t)\rangle$ is a sum of up to three exponentials.

$$\langle P_2(t)\rangle = a_0 + a_1\exp(-b_1 t) + a_2\exp(-b_2 t) + a_3\exp(-b_3 t) \quad (12)$$

Here the subscripts of a and b are different from those of Eq. (5) to distinguish between fitted and theoretical values. The determination of the $\langle P_2(t)\rangle$ function is model independent and a_i and b_i are expressed in terms of three parameters: the values of $\langle P_2\rangle$, $\langle P_4\rangle$ and the rotational diffusion coefficient of the probe in a isotropic medium with the same viscosity, $D_r^{\perp}$ [23,24]. The kinetics of the $\langle P_2(t)\rangle$ decay could be expressed by two characteristic relaxation times. One of them is the initial relaxation time, τ_{ini}, which describes the initial rate of decay can be expressed as [25]:

$$\tau_{ini} = (a_1 b_1 + a_2 b_2 + a_3 b_3)^{-1} = (6D_r^{\perp})^{-1} \quad (13)$$

and the other one is the mean relaxation time, τ_{mean}, that is given by

$$\tau_{mean} = (a_1/b_1 + a_2/b_2 + a_3/b_3)/(1 - a_0) \quad (14)$$

and is an indication of an average rate of a normalised decay along the whole curve.

The translational dynamics can be characterised by the mean square displacement of the probe's mass centre. For the co-ordinate α ($\alpha = x$, y or z) and for a time t the mean square displacement is given by $\langle[\alpha(t) - \alpha(0)]^2\rangle$, where the average is done over every possible choice of initial time. If the diffusion is free, in an unlimited environment with no potentials acting on, a probe will have

$$\langle[\alpha(t) - \alpha(0)]^2\rangle = 2D_t t \quad (15)$$

where D_t is the isotropic translational diffusion coefficient. In the present case, it is expected that the lateral diffusion in directions x and y will obey to the latest expression. But the same will not be expected for the transversal diffusion in the z direction, since translation along this axis is confined by membrane surfaces and the enclosing potential. So, $\langle [z(t) - z(0)]^2 \rangle$ will have a different function of time. However, it was proved [25] that for short times ($t \to 0$) Eq. (15) will still be valid, because the probe would not be close enough, on the average, to the membrane surfaces, and it acts as it was in a free environment.

4. Results and discussion

4.1. Equilibrium properties

We present here the results of the application of Eqs. (8) and (9), for different magnitudes of potentials and membrane widths. The outcoming results from integration of Eqs. (8) and (9) were obtained using the Gauss method with as much as 60 points of quadrature.

Fig. 2 shows the angular distribution of the probe as we change the values of the system parameters. In Fig. 2a we can see how the angular distribution of the probe changes as we modify the membrane width, without any change in the remaining parameters of our system. We recall that the unit of length is the probe centre-to-center distance. It can be seen that the probe has less orientational freedom when the membrane is narrower and tending to be more vertical (along the transverse plane of the membrane), which is as expected. Fig. 2b shows the angular distribution of the probe as we change the lipophobic potential. With an increase of this potential the angular distribution of the probe becomes more strikingly bimodal, which is logical since a higher lipophobic potential pushes the lipophobic sphere of the probe further from the membrane interior. As the hydrophobic sphere motion is constrained by the membranes surfaces the result is a preference for more vertical orientations. Fig. 2c shows the angular distribution of the probe as we change the enclosing potential. There is not a great influence of this potential in the angular distribution of the probe though it is perceptible a slight decrease in the preference for more vertical orientations as the enclosing potential is increased.

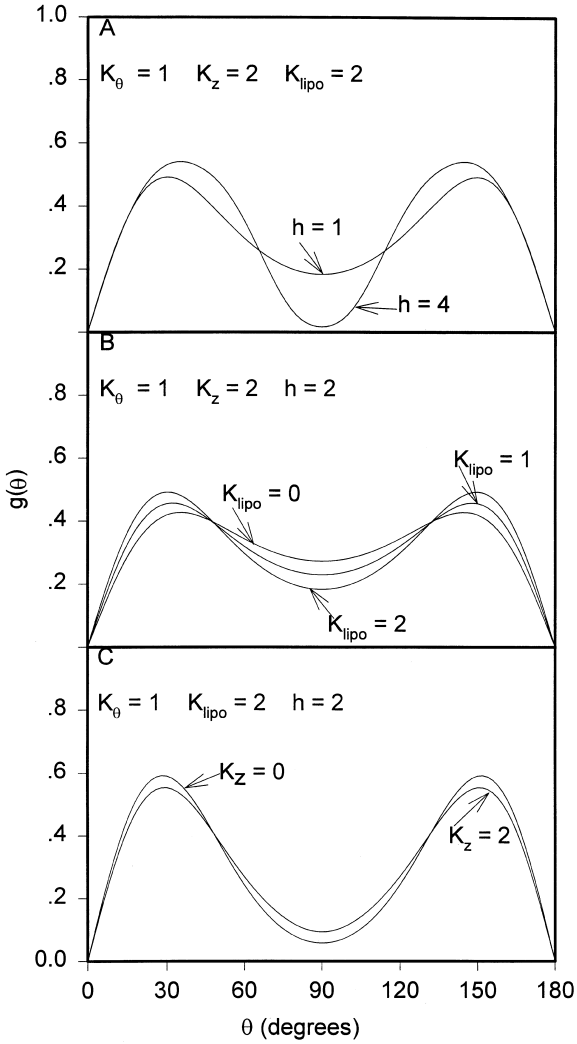

Fig. 2. Angular distribution, $g(\theta)$ vs. θ.

Fig. 3 shows the distribution of the hydrophobic sphere of the probe along the transverse plane of the membrane for different values of the system parameters. Fig. 3a presents the z distribution of the hydrophobic sphere when we change the membrane width. There is a striking alteration: the distribution goes from unimodal to a clear bimodal distribution. These results suggest that the flip-flop movements in a membrane are rota-

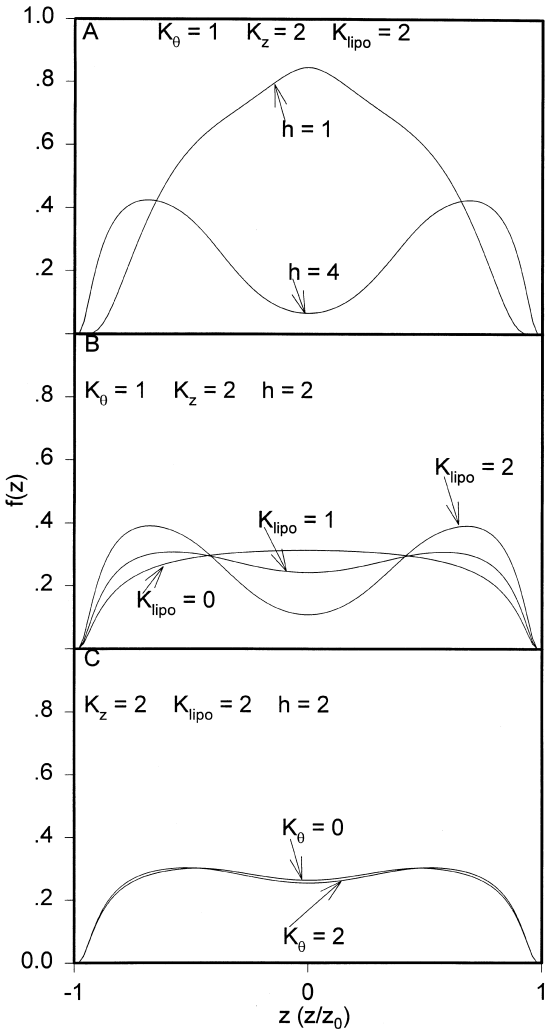

Fig. 3. Distribution function $f(z)$ vs. z/z_0 ($z_0 = h/2$).

tional rather than translational, for molecules which possess just about the same length as the membrane width. Fig. 3b shows the z distribution of the hydrophobic sphere of the probe as we change the lipophobic potential. As it can be seen an increase in the lipophobic potential has an effect of shifting the hydrophobic sphere of the probe closer to the membrane surfaces, which is logical. In Fig. 3c we show how the z distribution of the hydrophobic sphere of the probe varies as we change the orientational potential. There is no meaningful alteration in the distribution profile a clear indication that the orientational potential does not contribute much for the z distribution of the hydrophobic sphere of the probe.

It is interesting to study the case when there are no applied potentials, meaning $K_\theta = 0$, $K_z = 0$ and $K_{\text{lipo}} = 0$. In this case, Eqs. (8)–(10) can be solved analytically. Focusing our attention on Eq. (10) we will arrive to a result of $\langle \cos^2\theta \rangle = 1/3$ and consequently $\langle P_2(\cos\theta)\rangle = 0$. This result is independent of the membrane width. We may compare this result with the one obtained for a hydrophobic dimer enclosed in a membrane in the absence of applied potentials, by Huertas et al. [25]. In the case of a amphipathic dimer there is no rotational restriction though the hydrophobic sphere ought to remain in the interior of a membrane. This means that for any position of the hydrophobic sphere there is an absolute rotational freedom. Conversely, in the case of a hydrophobic dimer there is not a complete rotational freedom. The rotational motion is restricted by the surfaces of the membrane because both spheres are hydrophobic. It is clear that when $h/l \to \infty$, meaning infinite membrane width, the order parameter value, $S = \langle P_2(\cos\theta)\rangle$, of the hydrophobic dimer will approach the order parameter value of the amphipathic dimer.

Table 1 has the results of the equilibrium values of $\langle P_2(\cos\theta)\rangle$ and $\langle P_4(\cos\theta)\rangle$ obtained from the simulated trajectories and the theoretical ones. For the determination of error, the trajectory was divided into a few subtrajectories. From each subtrajectory we determine the mean value of the property in question. The value shown in the table is the mean of the property for each set of subtrajectories and the error is given by

$$\text{Error} = 1/\sqrt{n} * \sigma$$

where n is the number of subtrajectories and σ is the standard deviation of the mean.

As it is shown theoretical and simulated values agree within statistical error in all cases. It is noteworthy that $\langle P_4(\cos\theta)\rangle$ is generally quite small, and therefore, the simulation errors are relatively more important than for $\langle P_2(\cos\theta)\rangle$.

One can see that increasing the value of the lipophobic potential induces an increase in the order parameter value of the system. This is due

Table 1
$\langle P_2(\cos\theta)\rangle$ and $\langle P_4(\cos\theta)\rangle$ theoretical values and values obtained from simulated trajectories

h	K_θ	K_z	K_{lipo}	$\langle P_2(\cos\theta)\rangle$		$\langle P_4(\cos\theta)\rangle$	
				Simulation	Theory	Simulation	Theory
4	1	1	0	0.19 ± 0.05	0.220	0.01 ± 0.03	0.032
4	1	1	1	0.19 ± 0.05	0.243	0.02 ± 0.03	0.038
4	1	1	2	0.24 ± 0.05	0.269	0.03 ± 0.03	0.044
4	1	1	3	0.25 ± 0.05	0.295	0.04 ± 0.03	0.050
4	1	1	4	0.28 ± 0.05	0.317	0.04 ± 0.03	0.055
2	1	0	3	0.30 ± 0.05	0.316	0.03 ± 0.03	0.054
2	1	1	3	0.36 ± 0.04	0.397	0.05 ± 0.03	0.063
2	1	2	3	0.40 ± 0.04	0.425	0.05 ± 0.02	0.068
2	1	3	3	0.42 ± 0.04	0.443	0.05 ± 0.02	0.073
4	0	1	1	0.00 ± 0.05	0.020	0.00 ± 0.02	0.000
4	1	1	1	0.19 ± 0.05	0.243	0.02 ± 0.03	0.038
4	2	1	1	0.43 ± 0.05	0.458	0.12 ± 0.03	0.136
4	3	1	1	0.59 ± 0.04	0.617	0.02 ± 0.02	0.258
1	1	4	4	0.37 ± 0.04	0.381	-0.01 ± 0.02	0.002
2	1	4	4	0.40 ± 0.04	0.423	0.04 ± 0.02	0.068
4	1	4	4	0.28 ± 0.05	0.317	0.04 ± 0.03	0.055

probably to the fact that the probe tends to stay with higher probability with a vertical orientation as it can be hinted from Fig. 2.

The same thing happens when we increase the enclosing potential. In other words, the hydrophobic sphere tends to stay further away from the membrane surfaces and this is achieved we a more vertical orientation of the probe, inducing an increase in the order parameter value. Obviously, an increase in the orientational potential has a striking effect of increasing the order parameter values of our system.

4.2. Dynamic properties

It is of great interest to watch the evolution of the lipophobic sphere trajectory along the transverse plane of the membrane in our simulations. This gives an idea of the motion of the probe in our system. Figs. 4–6 display examples of trajectories in the z direction for distinct situations.

For instance, Fig. 4 shows how the trajectory of this sphere evolves as we change the membrane width. Increasing the membrane width from 2 to 4, without any changes in other parameters, has the effect of reducing the number of flip-flop movements. This is not surprising since the probe has to travel a longer distance in the membrane, with the consequent longer exposure to the lipophobic potential that tends to drive it to the membrane surface. So, the probe tends to stay in the vicinity of only one of the membrane surfaces.

Fig. 5 displays the trajectories of the lipophobic sphere of the probe as we change the lipophobic potential. We can see that an increment in this potential, remaining the other parameters of our system unaltered, produces a decrease in the number of flip-flop movements. The interpretation is quite straightforward since an increase in the lipophobic potential has a direct consequence of pushing the lipophobic sphere towards the membrane surfaces and making difficult it's presence in the interior of the membrane.

Fig. 6 reproduces the motion of the lipophobic sphere in our system when we change the enclosing potential, without any alteration in the other parameters. It can be seen that the only significant alteration is the fact that when this sphere gets out of the membrane tends to stay closer to the membrane surface as we increase the enclosing potential. This is explained by the fact that a higher enclosing potential will not let the hy-

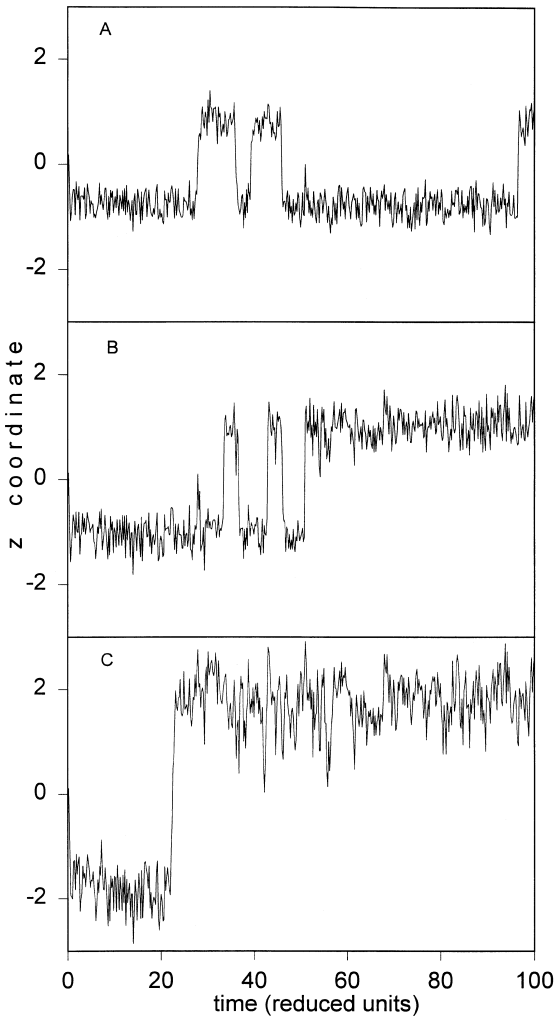

Fig. 4. Evolution of z along a portion of a BD trajectory of 100 units of reduced time with the following system parameters: (a) $h = 1$; (b) $h = 2$; (c) $h = 4$. In all situations $K_\theta = 1$, $K_z = 1$, $K_{\text{lipo}} = 4$.

drophobic sphere to get close to the membrane surface, restraining in this way the motion of the probe.

A similar study (not shown), varying the magnitude of the orientational potential, remaining the other parameters of our system fixed, was performed. It was found that the increase of the magnitude of the orientational potential has the effect of allowing the lipophobic sphere to get a little further out of the membrane. The basis of this effect is the fact that a higher orientational potential favours a more vertical (parallel to the transverse plane of the membrane) orientation of the probe. This way when the hydrophobic sphere reaches the membrane surfaces the lipophobic sphere can be more distant from them along the z direction.

Examples of the results of the analysis of rotational dynamics are presented in Fig. 7, where are shown $\langle P_2(t^*)\rangle$ decays for different magnitudes of our system parameters. The full lines represent the theoretical values calculated by means of Eq.

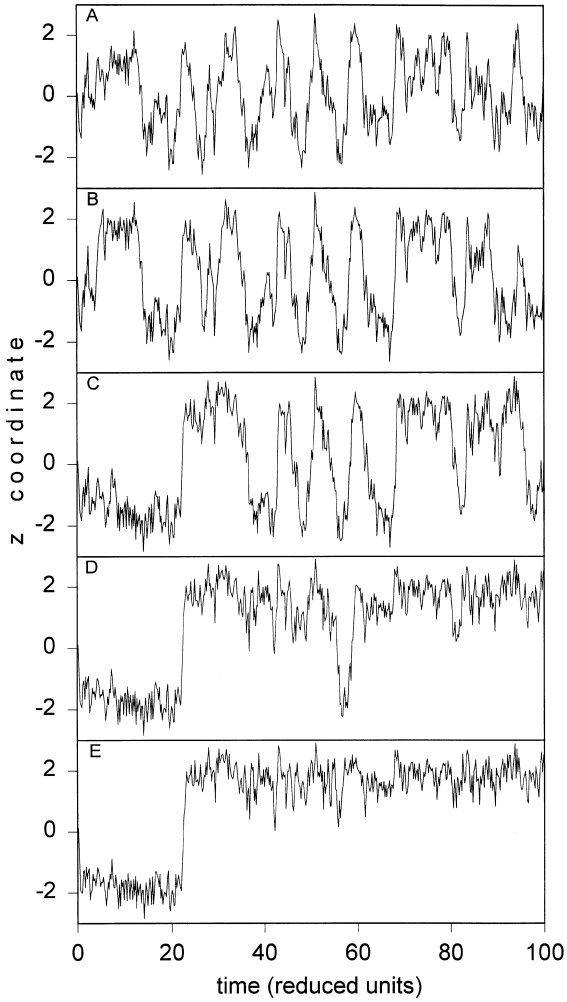

Fig. 5. Evolution of z along a portion of a BD trajectory of 100 units of reduced time with the following system parameters: (a) $K_{\text{lipo}} = 0$; (b) $K_{\text{lipo}} = 1$; (c) $K_{\text{lipo}} = 2$; (d) $K_{\text{lipo}} = 3$; (e) $K_{\text{lipo}} = 4$. In all situations $K_\theta = 1$, $K_z = 1$, $h = 4$.

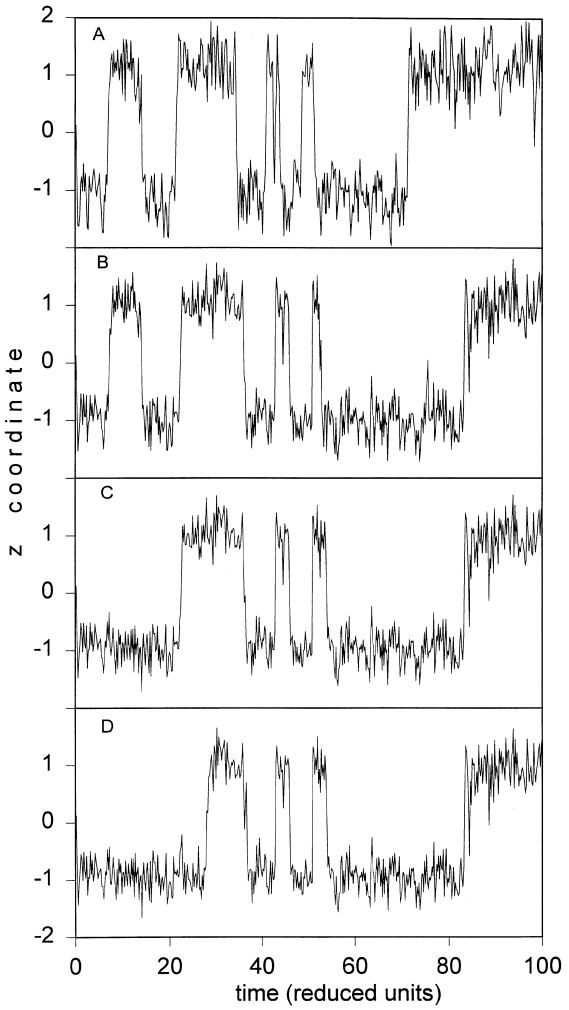

Fig. 6. Evolution of z along a portion of a BD trajectory of 100 units of reduced time with the following system parameters: (a) $K_z = 0$; (b) $K_z = 1$; (c) $K_z = 2$; (d) $K_z = 3$. In all situations $K_\theta = 1$, $K_{\text{lipo}} = 3$, $h = 2$.

(12) and the dashed lines the values resulting from Brownian dynamics simulation. There is a good agreement between the model-free theoretical values and the values outcoming from simulation. The *plateau* values of $\langle P_2(t^*)\rangle$, which should be $\langle P_2\rangle^2$, are equal to those reproduced in Table 1. The values of $D_r^{\perp}$ extracted from the fitting curves to the simulated $\langle P_2(t^*)\rangle$ decays, according to Eq. (13), are in agreement with the theoretical value for the free-diffusion isotropic $D_r^{\perp}$, with deviations smaller than 5%.

An example of the analysis of translational dynamics is shown in Fig. 8. It can be seen that the translational displacement is in agreement with theoretical predictions [25], meaning that in the unbounded direction has a linear behaviour and that in the limited direction it has an asymptotic behaviour. Nevertheless, a short time analysis allowed us to extract the values of translational diffusion coefficient, after a fit performed according to Eq. (15), in the cases of limited or unbounded translation. The extracted values are in excellent agreement with the theoretical values for the free particle diffusion, with deviations in the order of 2%.

These two last results are a strong evidence of the validity of Brownian dynamics simulation in the prediction of rotational and translational properties of molecules.

5. Conclusions

The representation of a membrane features such as order and amphipathic nature by poten-

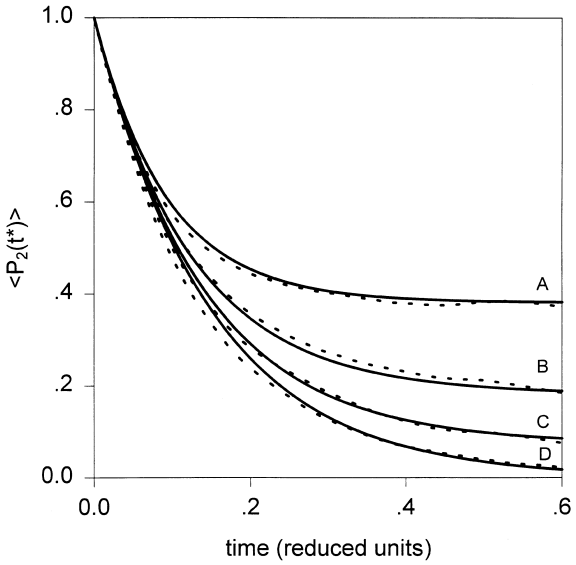

Fig. 7. Decay of correlation function $\langle P_2(t^*)\rangle$ with reduced time. Solid curves are theoretical approximation and dotted curves simulation results for the following system parameters: (a) $K_\theta = 1$, $K_z = 1$, $K_{\text{lipo}} = 3$, $h = 2$; (b) $K_\theta = 0$, $K_z = 1$, $K_{\text{lipo}} = 1$, $h = 4$; (c) $K_\theta = 1$, $K_z = 0$, $K_{\text{lipo}} = 0$, $h = 500$; (d) $K_\theta = 1$, $K_z = 1$, $K_{\text{lipo}} = 1$, $h = 4$.

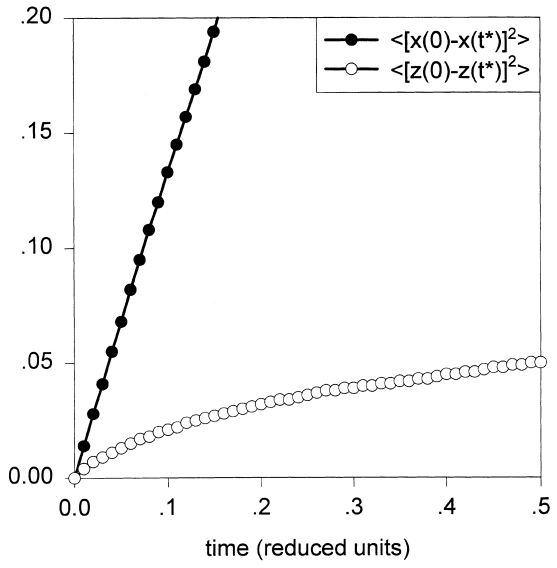

Fig. 8. Translational correlation functions $\langle [x(t)-x(0)]^2 \rangle$ and $\langle [z(t)-z(0)]^2 \rangle$ vs. reduced time with the following system parameters $K_\theta = 1$, $K_z = 1$, $K_{\text{lipo}} = 1$, $h = 4$.

tials allowed us to build a simple model that still provides all important predictions about the behaviour of probes positioned in a membrane. The simplicity of the model enables an accurate foresight of equilibrium properties of a probe such as angular distributions, distributions along the transverse plane of the membrane and order parameters.

The prediction of dynamic properties of the probe is also achieved with this model and we can extract relevant information from Brownian dynamics simulation, such as $P_2(t)$ decays that might be confronted with experimental results of spectroscopic techniques. The rotational dynamic behaviour of the probe agrees reasonably well with the predictions of the so called model-free theoretical approach [23,24], in spite of the complexity of our system.

The translational behaviour an amphipathic probe was found to be consistent with the theoretical predictions of Huertas et al. [25] for a similar case.

We can also conclude that the rotational behaviour of an amphipathic probe is not strongly influenced by the membrane width though the translational behaviour is, as it can be ascertained, for instance, by the dependence of flip-flop movements on membrane width. This is different from the results of an hydrophobic probe which is greatly influenced by the membrane width.

In the present work, the embedded probe molecule has been simply modelled as a dumbbell, so that the application to a specific probe-membrane system still requires a parameterization step to assign values to σ_1, σ_2, l, etc. We also foresee the possibility of incorporating molecular detail (atoms, bonds, etc.) in the model of the probe. Whatever the level of specification or detail is, the Brownian dynamics simulation appears as a powerful tool for the prediction of equilibrium properties, translational and rotational behaviour of molecules positioned in a membrane, and allows the analysis of the influence of the various aspects of the interaction of the molecule with the membrane environment.

Acknowledgements

We thank Fundação para a Ciência e Tecnologia (Portugal) for grant PRAXIS XXI BD/9393/96 to MXF, Dirección General de Enseñaza Superior (Spain) for grant PB 96–1106 and for a predoctoral fellowship to MLH, grant CI1*CT940124 from the Comission of the European Community, and grant 01758/CV/98 from Fundación Séneca.

References

[1] B.R. Lentz, in: L.M. Loew (Ed.) Spectroscopic Membrane Probes, CRC, Boca Raton, Florida, USA, 1988, Ch. 2.
[2] C. R Mateo, P. Lillo, J.C. Brochon, M. Martinez-Ripoll, J. Sanz-Aparicio, A.U. Acuña, J. Phys. Chem. 97 (1993) 3486.
[3] C.R. Mateo, J.C. Brochon, M.P. Lillo, A.U. Acuña, Biophys. J. 65 (1993) 2237.
[4] C.R. Mateo, P. Tauc, J.C. Brochon, Biophys. J. 65 (1993) 2248.
[5] C.R. Mateo, A.U. Acuña, J.C. Brochon, Biophys. J. 68 (1995) 978.
[6] C.R. Mateo, A.A. Souto, F. Amat-Guerri, U.A. Acuña, Biophys. J. 71 (1996) 2177.
[7] P.M. Bayley, R. Dale (Eds.), Spectroscopic and the Dynamics of Molecular Biological Membranes, Academic, New York, USA, 1985.

[8] P.H. Devaux, M. Seigneuret, Biochim. Biophys. Acta. 822 (1985) 63.
[9] D.S. Cafiso, Annu. Rev. Biophys. Biomol. Struct. 23 (1994) 141.
[10] K. Belohorcova, J.H. Davis, T.B. Woolf, B. Roux, Biophys. J. 73 (1997) 3039.
[11] S. Jayasinghe, M. Barranger-Mathys, J.F. Ellena, C. Franklin, D.S. Cafiso, Biophys. J. 74 (1998) 3023.
[12] P. van der Ploeg, H.J.C. Berendsen, J. Chem. Phys. 76 (1982) 3271.
[13] J.J. Lopez Cascales, J. García de la Torre, S.J. Marrink, H.J.C. Berendsen, J. Chem. Phys. 104 (1996) 2713.
[14] D.P. Tieleman, S.J. Marrink, H.J.C. Berendsen, Biochim. Biophys. Acta. 1331 (1997) 235.
[15] J.J. Lopez Cascales, H.J.C. Berendsen, J. García de la Torre, J. Phys. Chem. 100 (1996) 8621.
[16] J.J. Lopez Cascales, J. García de la Torre, Biochim. Biophys. Acta 1330 (1997) 145.
[17] J.J. Lopez Cascales, J.G. Hernandez Cifre, J. García de la Torre, J. Phys. Chem. 102 (1998) 625.
[18] J.J. Lopez Cascales, M.L. Huertas, J. García de la Torre, Biophys. Chem. 69 (1997) 1.
[19] D.H. Bassolino-Klimas, H.E. Alper, T.R. Stouch, Biochemistry 32 (1993) 12624.
[20] R.W. Pastor, R.M. Venable, J. Chem. Phys. 89 (1988) 1112.
[21] R.W. Pastor, R.M. Venable, M. Karplus, A. Szabo, J. Chem. Phys. 89 (1988) 1128.
[22] R.W. Pastor, R.M. Venable, in: W. van Gunsteren, P.K. Weiner, A.K. Wilkinson (Eds.), Computer Simulations of Biomolecular Systems: Theoretical and Experimental Applications, ESCOM Science Publishers, Leiden, The Netherlands, 1994.
[23] A. Szabo, J. Chem. Phys. 81 (1984) 150.
[24] W. van der Meer, H. Pottel, W. Herreman, M. Ameloot, H. Hendricks, H. Schroder, Biophys. J. 46 (1984) 525.
[25] M.L. Huertas, V. Cruz, J.J. Lopez Cascales, A.U. Acuña, J. Garcia e la Torre, Biophys. J. 71 (1996) 1428.
[26] C.W. Oseen. Hydrodynamik, Academisches Verlag, Leipzig, 1927.
[27] J. García de la Torre, V.A. Bloomfield, Q. Rev. Biophys. 14 (1981) 81.
[28] J. García de la Torre, V. Rodes, J. Chem. Phys. 79 (1983) 2454.
[29] D.L. Ermak, J.A. McCammon, J. Chem. Phys. 69 (1978) 1352.
[30] A. Iniesta, J. García de la Torre, J. Chem. Phys. 92 (1990) 2015.
[31] S. Provencher, J. Chem. Phys. 89 (1976) 1128.
[32] S. Provencher, Biophys. J. 16 (1976) 151.